

Striving Towards Noble-Metal-Free Photocatalytic Water Splitting: The Hydrogenated-Graphene-TiO₂ Prototype

Thuy-Duong Nguyen-Phan,¹ Si Luo,^{1,2} Zongyuan Liu,^{1,2} Andrew D. Gamalski,³ Jing Tao,⁴ Wenqian Xu,¹ Eric A. Stach,³ Dmitry E. Polyansky,¹ Sanjaya D. Senanayake,¹ Etsuko Fujita¹ and José A. Rodríguez^{1*}

¹ Chemistry Department, ³ Center for Functional Nanomaterials, ⁴ Condensed Matter Physics and Materials Science Department, Brookhaven National Laboratory, Upton, NY 11973, United States

² Department of Chemistry, Stony Brook University, Stony Brook, NY 11790, United States

KEYWORDS *Titania, reduced titania, hydrogenated graphene, graphene, turbostratic carbon, water splitting, hydrogen production.*

ABSTRACT: Graphane, graphone and hydrogenated graphene (HG) have been extensively studied in recent years due to their interesting properties and potential use in commercial and industrial applications. The present study reports investigation of hydrogenated graphene/TiO_{2-x} (HGT) nanocomposites as photocatalysts for H₂ and O₂ production from water without the assistance of a noble metal co-catalyst. By combination of several techniques, the morphologies, bulk/atomic structure and electronic properties of all the powders were exhaustively interrogated. Hydrogenation treatment efficiently reduces TiO₂ nanoparticles, while the graphene oxide sheets undergo the topotactic transformation from a graphene-like structure to a mixture of graphitic and turbostratic carbon (amorphous/disordered) upon altering the calcination atmosphere from a mildly reducing to a H₂-abundant environment. Remarkably, the hydrogenated graphene-TiO_{2-x} composite that results upon H₂-rich reduction exhibits the highest photocatalytic H₂ evolution performance equivalent to low loading of Pt (~0.12 wt%), whereas the addition of HG suppresses the O₂ production. We propose that such an enhancement can be attributed to a combination of factors including the introduction of oxygen vacancies and Ti³⁺ states, retarding the recombination of charge carriers and thus, facilitating the charge transfer from TiO_{2-x} to the carbonaceous sheet.

INTRODUCTION

Since the discovery in 2004 by Novoselov et al.,^{1,2} graphene (GP), called the “mother of all graphitic forms”, has attracted considerable attention due to its unique structure, outstanding properties and potential for use in commercial and industrial applications including electronics, mechanical devices, catalysis and energy conversion. Tremendous efforts have been devoted to fabrication of the nanoassemblies of metal oxide and GP and its derivatives (graphene oxide - GO, reduced graphene oxide - RGO) for further potential applications.³⁻⁹ Among several systems containing a metal oxide and graphene, GP/TiO₂ composites have been reported to be highly promising, visible-light-responsive photocatalysts, active for processes such as wastewater treatment, air purification, solar water splitting, self-cleaning surfaces and CO₂ reduction. The origin of such properties is largely due to simultaneously enhanced adsorption capacity, extended light absorption, superior stability and excellent electron transport.¹⁰⁻²¹

TiO₂ is the most widely used photocatalyst with a high propensity for generating pairs of electrons and holes upon photon absorption.^{22,23} A noteworthy obstacle is that

both the rapid recombination of these charge carriers within nanoseconds and the limited absorption in the near-UV region renders diminished either efficiency or activity of the photocatalytic reaction and partially limits its wide use in practical applications. The combination of TiO₂ with graphene efficiently overcomes these barriers due to its multifunction as an additional adsorbent, electron acceptor and transporter, stabilizer and photosensitizer.¹⁰⁻²¹ GP sheets efficiently suppress the recombination of photoinduced electron-hole pairs, accelerate the transfer of electrons, enhance the surface-adsorbed quantity of target molecules via π - π and electrostatic interactions, as well as extend the absorption range to the visible light region by either narrowing the band gap or introducing an additional gap.¹⁰⁻²¹

Despite the fact that a cornucopia of scientific studies devoted to GP/TiO₂ composite materials has been reported, our fundamental understanding of these materials appears to have reached a plateau. Meanwhile, combining TiO₂ with fully hydrogenated graphene (known as ‘graphane’) or partially/half-hydrogenated graphene (as ‘graphone’) has not been achieved and remains at the forefront of photoelectrochemical research. Graphane,

graphone or hydrogenated graphene (HG), where the GP's aromatic bonds are saturated with hydrogen atoms by high pressure hydrogenation, low pressure hydrogen plasma and wet chemistry (Birch reduction), have been considered as promising semiconductor materials and as an efficient, stable support for anchoring metal/metal oxide catalysts.²⁴⁻³¹ Due to the attachment of the atomic hydrogen to each site of the atomic scaffold of the GP lattice, the hybridization of carbon atoms alters the matrix from sp^2 to sp^3 , hence removing the conducting π -bands and opening an energy gap.²⁴ Upon hydrogenation of a honeycomb graphene lattice, three conformations of graphane can be generated, including chair, boat and washboard conformations, and each conformer is characterized by a specific hydrogen sublattice and by a different buckling of the carbon sublattice.²⁶ The C-C bond lengths in graphane and graphone are different from graphene.^{25,26,28} Such hydrogenated graphene (HG) materials exhibit ferromagnetism and more importantly, its band gap is readily tunable, depending on the extent of hydrogenation. When half of the hydrogen in the graphane sheet is removed, the resulting semi-hydrogenated graphone or graphone becomes a ferromagnetic semiconductor with a small indirect gap arising from the formation of strong σ -bonds and the breakage of the delocalized π -bonding network of GP, leaving the electrons in the unhydrogenated carbon atoms localized and unpaired.²⁵ Notably, graphone is very different from graphane, with a large direct band gap and also in comparison to GP, which has a zero band gap. Up to now, there are few experimental studies devoted to either graphane and graphone.^{24,27,30}

It is important to emphasize here that the introduction of hydrogen species by either physical or chemical methods not only successfully produces such a GP-like family of materials but also imparts a modification to the reduced titania (TiO_{2-x}) with a sub-stoichiometric Ti:O ratio. The coloration of TiO_2 (red, yellow, blue, grey, black) has sparked increasing research interest in recent years with the promise of overcoming the challenges of purely white TiO_2 itself.³²⁻³⁷ The synthesis and functionality of such nanomaterials have been a very promising approach, not only to drastically enhance the activity by increasing the quantum efficiency but also to extend the optical absorption into the visible region by introducing a substantial amount of lattice disorder or defects.³²⁻³⁴

In the light of these facts, investigating the hydrogen coverage via the extent of hydrogenation, on the coupling of TiO_{2-x} with hydrogenated graphene, graphone or graphane is a promising approach that possibly exhibits strong impact on the structural, physico-chemical, optical, electronic characteristics and even the catalytic activity of these materials. Wang et al.³⁸ synthesized hydrogenated TiO_2 -RGO via the hydrogenation of TiO_2 -graphite oxide at 450 °C for 4 h under a flowing atmosphere of 5% $\text{H}_2/95\%$ Ar. Such a composite was used as anode material in a high rate lithium ion battery, achieving a larger discharge capacity (234.3 mA h g^{-1}) than the composite reduced by hydrazine and subsequent annealed in nitrogen

atmosphere. Much higher reversible discharge capacity at a current rate of 5 C (up to 166.3 mA h g^{-1}), remarkable rate capability and outstanding cycling stability (2.4% capacity loss after 100 cycles) are attributed to the greatly improved electronic conductivity derived from hydrogenated TiO_2 (H- TiO_2), enhanced electron transport due to the role of reduced graphene as a conductive substrate, and the good contact between the zero-dimensional H- TiO_2 nanoparticles with two-dimensional (2D) RGO nanosheets. Very recently, Zhang and Chen³⁹ reported the influence of hydrogenation temperature for GO- TiO_2 composites on the photocatalytic degradation of Rhodamine B. The highest photocatalytic activity was obtained by the hybrid material prepared at 450 °C due to the formation of p-n junctions and appropriate charge mobility.

Given these many aspects, we have endeavored to systematically investigate in this study the influence of hydrogenation extent on the structural, physico-chemical and electronic properties of hydrothermal-prepared GO- TiO_2 composites. The impact of this structure on the light-driven O_2 and H_2 production from water without the assistance of noble metal co-catalyst (*i.e.* Pt, Ru, Rh) was interrogated and the role of individual components in the overall photocatalytic reaction was proposed. Otherwise, one should bear in mind that due to the high cost and frequent scarcity of Pt in Earth's crust, its use has been strictly controlled and herein, hydrogenated graphene- TiO_{2-x} composites were benchmarked against the well-known Pt/ TiO_2 system, demonstrating the potential of new noble-metal-free catalysts to replace expensive and non-abundant metals in terms of economics, abundance, environmental considerations and catalytic effectiveness.

EXPERIMENTAL

Synthesis of materials

The GO dispersion (3.5 mg mL^{-1}) was synthesized by a modified Hummers method and the detailed preparation is described in the Supporting Information. In a typical procedure, 7 mL titanium *n*-butoxide and 1 mL hydrochloric acid (35 wt%) were loaded into a Teflon-line stainless steel autoclave and statically aged at 150 °C for 6 h. After cooling to room temperature, the white precipitate was washed by ethanol and centrifuged at 15000 rpm and re-dispersed into ethanol. The *as-syn* TiO_2 was obtained by freeze-drying the product after washing and centrifugation. A desired amount of GO dispersion (1 wt%) was

Table 1. Structural parameters from N_2 sorption^a, XRD^b, and Raman^c analyses.

Samples	Surface area / $\text{m}^2 \text{g}^{-1}$ ^a	Crystallite size / nm ^b	Lattice parameters / Å ^b		Peak intensity ratio I_D/I_G ^c
			$a = b$	c	
TiO_2	47.5	14.19	3.7858	9.5106	-
$\text{TiO}_{2-x}@H_2$	56.6	13.10	3.7855	9.5089	-
HGT@ H_2 /Ar	123.3	9.17	3.7877	9.5100	1.53
HGT@ H_2	74.9	12.10	3.7885	9.5165	1.26

added into TiO₂-ethanol dispersion under vigorous stirring at room temperature for 30 min. After sonicating for 30 min, the mixture was hydrothermally treated at 80 °C for 4 h. Subsequent to washing with deionized water, the product was lyophilized and hydrogenated at 500 °C for 4 h. The final composites were then annealed in two environments: (i) hydrogen-argon mixture (15% H₂/85% Ar), and (ii) ultra-high-purity H₂, denoted as HGT@H₂/Ar and HGT@H₂, respectively.

For comparison, hydrogen-reduced titania was also prepared by the same procedure without the addition of GO and named as TiO_{2-x}@H₂. Other control samples include nanosized anatase calcined in ambient air (TiO₂) and GO annealed in pure H₂ (HG@H₂).

Characterizations

X-ray diffraction (XRD) patterns and pair distribution function (PDF) profiles were collected at beamline X7B ($\lambda = 0.3196 \text{ \AA}$) of the National Synchrotron Light Source (NSLS) at Brookhaven National Laboratory (BNL). The powder samples (5 mg) were loaded into a 0.9-mm-ID quartz capillary and the two-dimensional diffraction patterns were collected by a Perkin Elmer amorphous silicon detector. The raw data were integrated by Fit2D code (calibrated by LaB₆ standard) while the crystalline phase identification, composition and lattice parameters were subsequently analyzed by Rietveld refinement using General Structure Analysis System (GSAS) program.⁴⁰ PDF data processing was subsequently performed with Python/PDFgetX3 to describe the distribution of all pairs of atoms within a sample as a function of interatomic distance.

High-resolution X-ray photoemission spectra were collected at beamline U12A of the NSLS at BNL examining the Ti 2p, C 1s and O 1s core level regions. The probing depth for 700 eV-photon energy was 8 nm and the data were further processed by CASAXPS.

Further characterization of the materials was also conducted using several techniques available at the Center for Functional Nanomaterials (CFN) at BNL. Scanning electron microscopy (SEM) was carried out by a Hitachi S-4800. Transmission electron microscopy (TEM) images were recorded on a FEI Titan 80-300 with an objective-lens aberration corrector and a field-emission gun operating at 300 kV. The powder samples were dispersed in water by sonication and dropped onto a carbon film coated copper grid and air dried overnight. Raman spectroscopy was performed on WiTec Alpha combination microscope at room temperature with 633 nm laser as an excitation source. UV-vis diffuse reflectance (DRS) measurements were collected at room temperature by PerkinElmer Lambda 950 spectrometer equipped with an integrating sphere assembly.

Brunauer-Emmett-Teller (BET) specific surface areas were determined by N₂ adsorption/desorption at 77 K using an Altimira AMI-300ip instrument at Stony Brook University. The powders were degassed at 150 °C to remove all surface-adsorbed contaminants prior to measurements. Solid state ¹H nuclear magnetic resonance

(NMR) spectroscopy was conducted on a Bruker Advance III, operating at 500 MHz at room temperature. The magic angle spinning (MAS) frequency was 12 kHz and one-dimensional spectra were acquired with 16 scans. ¹H chemical shifts were externally referenced to adamantane and NMR data were further processed using TopSpin 3.1.

Photocatalytic water splitting measurements

The photocatalytic water splitting activity was evaluated through the measurement of either hydrogen or oxygen evolution in a closed gas circulation and evacuation system. The aqueous methanol solution (20 vol%) and 0.01 M AgNO₃ were used as sacrificial agents to probe the H₂ and O₂ gas evolution, respectively, in separated experiments. The reactor was side-irradiated by a 150 W Xe arc lamp from Optical Building Blocks Corporation which utilizes elliptical reflector (F = 379 mm) and equipped with CuSO₄ filter (310 nm < λ < 625 nm, see in Fig. S1 – Supporting Information). The lamp was placed in the focal point of the lamp and the light intensity was 750 mW over an irradiated area of 1.13 cm² which was measured by an optical power meter (Ophir Optronics). 400 nm long pass filter (Thorlabs, Inc.) was used to measure the activity under visible light illumination (light intensity 475 mW, 400 nm < λ < 625 nm). The detailed experimental conditions and procedures can be found in previous study.⁴¹ The evolved gases were determined by gas chromatography (GC Agilent 6890N) equipped with FID and TCD detectors using Ar as the carrier gas. The apparent quantum efficiency (QE) was calculated according to the following equation:

$$\begin{aligned} \text{QE} [\%] &= \frac{\text{number of reacted electrons}}{\text{number of incident photons}} \times 100 \\ &= \frac{\text{number of evolved H}_2 \text{ molecules} \times 2}{\text{number of incident photons}} \times 100 \end{aligned}$$

RESULTS AND DISCUSSION

Structural studies – XRD, PDF, Raman and ¹H NMR

The *as-syn* GO-TiO₂ composite was subsequently

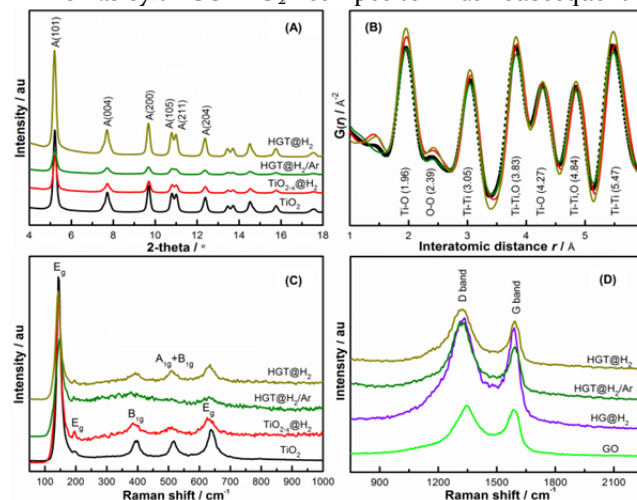


Figure 1. (A) XRD patterns, (B) PDF analysis and (C, D) Raman spectra of TiO₂, TiO_{2-x}@H₂ and HGT composites.

annealed at 500 °C for 4 h in two different atmospheres: (i) flow of 15% H₂ in Ar and (ii) ultra-high-purity H₂ (both under 20 psi), to investigate the effectiveness of hydrogenation on the structural, physico-chemical, electronic properties and photocatalytic performance. The crystallographic structures of HGT composites and other reference materials were confirmed by synchrotron XRD patterns displayed in Fig. 1A. In all samples, series of well-defined (101), (004), (200), (105), (211) and (204) diffraction peaks are indexed to the tetragonal anatase (space group *I*₄*/amd*) without any trace of rutile. Herein, the crystallinity decreases due to the evolution of hydrogen gas, leading to the formation of defects that inhibit the crystal growth of TiO_{2-x}, except for HGT@H₂. Notably, a lack of diffraction peaks representative of the carbonaceous component can possibly be explained by the exfoliation of GO nanosheets during synthesis, the intercalation of TiO₂ particles or the shielding of the (002) carbon-like feature by the strong (101) diffraction of anatase TiO₂.^{10,11,14,17} The crystalline phase, particle size and unit cell parameters were determined by Rietveld refinement and summarized in Table 1. As seen in Fig. S2 (Supporting Information) and Table 1, annealing in an H₂ atmosphere clearly causes a lattice distortion in both TiO_{2-x}@H₂ and HGT composites. Particularly, a lattice expansion is found on HGT composites whereas the shrinkage occurs on TiO_{2-x}@H₂. The average crystallite size remarkably increases from 6 nm to 9-13 nm under a reducing atmosphere compared to TiO₂. It can be seen that the lack of oxygen in the H₂-reducing environment efficiently aggravates the deformation of the unit cell and restrains the grain growth during calcination.

In addition, the PDF signal takes into account all components of the XRD pattern and contains all characteristic interatomic distances in the materials. The corresponding PDF profile in Fig. 1B points to numerous well-defined maxima at 1.96, 2.39 and 3.05 Å that are ascribable to the mean bond lengths of Ti-O, O-O and Ti-Ti pairs for the first neighbor coordination shell of [TiO₆] octahedra (the closest O shell around a Ti atom). Note that each Ti ion in the anatase structure octahedrally coordinates to six O ions with an atypical Ti-O bond length of 1.98 Å and an equatorial bond length of 1.93 Å.⁴¹ The peaks at 3.83 Å represents the second asymmetric Ti-Ti,O coordination sphere. No apparent differences are encountered among these samples except the shift to a larger interatomic distance and the alteration in maxima intensity upon hydrogenation, implying the distortion of [TiO₆] octahedra. Apart from the distances less than 6 Å – considerable short- and medium-range order, the longer correlation up to 20 Å in Fig. S3 (Supporting Information) clearly demonstrates the absence of long-range order, indicating the surface disorder or structural distortion by hydrogenation.

Raman spectroscopy, a non-destructive method, is also a useful technique to explore the crystalline or molecular changes after hydrogenation via molecular vibrations. Fig. 1C shows several characteristic Raman-active modes at 145

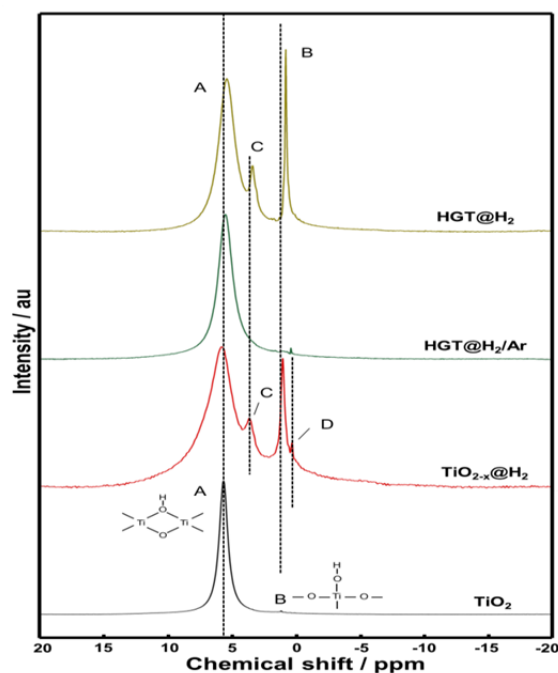


Figure 2. Solid state ¹H NMR, of TiO₂, TiO_{2-x}@H₂ and hydrogenated graphene/TiO_{2-x} composites.

(E_g), 198 (E_g), 398 (B_g), 516 (A_g+B_g) and 638 (E_g) cm⁻¹ for TiO₂, identifying the tetragonal structure of anatase TiO₂, which is consistent with XRD and TEM observations. These modes become weakened and broaden together with the emerging of numerous smaller, weaker bands for either TiO_{2-x}@H₂ or HGT composites after H₂ reduction, stemming most likely from the surface heterogeneity or disorder that may activate zone-edge and otherwise Raman-forbidden modes by breaking down the Raman selection rules.^{32,43} The results in our study are consistent with previous reports which claim that the introduction of H₂ induced the spreading and impairment of these indicative bands, implicating hydrogenation-induced structural changes at the surface.³²⁻³⁴ Moreover, the formation of intrinsic defects is one of the possible reasons for Raman mode broadening because as they scatter phonons, causing their decay and consequent decrease in their lifetime, resulting in an increase in the phonon line width.^{44,45}

Raman spectroscopy can also be utilized to identify either *sp*²-*sp*³ hybridized carbon atoms or disorder/defects in HG composites. As illustrated in Fig. 1D, two typical D and G bands are observed in both samples. The D band at 1350 cm⁻¹ is assigned to the vibration of carbon atoms with the *sp*³ electronic configuration of disordered graphene or *sp*³ defects near K-point, whereas the G band at 1587 cm⁻¹ is associated with the in-plane vibration of *sp*²-bonded carbon atoms at the Γ-point and a doubly-degenerated phonon mode (E_{2g} symmetry) at the Brillouin zone center.^{13,46,47} The relative intensity ratio (I_D/I_G) is usually calculated to provide the information on the relative concentration of disorder or local defects in comparison with *sp*²-hybridized graphene domains. The I_D/I_G = 1.12 of HG

Table 2. ^1H NMR chemical shift^a and peak area ratios of C- and O-containing bonds obtained by XPS^b.

Samples	NMR chemical shifts ^a				XPS C 1s ^b		XPS O 1s ^b	
	A	B	C	D	[C-C/C-H]/C=C	%[C-C/C-H]	O _{II} /O _I	O _{III} /O _I
TiO ₂	5.63	1.18	-	-	-	-	0.277	0.182
TiO _{2-x} @H ₂	5.76	1.04	3.68	0.28	-	-	0.666	0.498
HGT@H ₂ /Ar	5.49	-	-	0.38	0.826	33.92	0.595	0.635
HGT@H ₂	5.35	0.83	3.44	-	1.155	39.74	0.760	0.221

annealed in H₂ is slightly higher than that of the GO precursor ($I_D/I_G = 1.05$), indicating a substantial decrease in sp^2 -bonded carbon atoms and oxidized molecular defects.⁴⁷ It is noteworthy that the integrated intensity significantly increases to 1.51 and 1.26 for HGT@H₂/Ar and HGT@H₂, demonstrating the formation of large amounts of edges, defects, disorders as well as abundant sp^3 C-H bonds and dense ripples after hydrogenation.⁴⁸ Interestingly, weaker signals are recorded for HGT@H₂, indicating that lower portion of graphitic structure or lower graphitization degree compared to HGT@H₂/Ar. The nature of the carbonaceous component was further investigated by TEM and XPS in the following section.

The solid state ^1H NMR spectroscopy was further conducted to characterize the hydrogen-containing species in the TiO₂, TiO_{2-x}@H₂ and HGT composites (Fig. 2). The chemical shifts of all resonances are shown in Table 2. A strong, sharp chemical shift at 5.63 ppm (resonance A) and very small peak at 1.18 ppm (resonance B) in TiO₂ are characteristic of the H at bridging and terminal sites.⁴⁹ Chary et al.⁵⁰ ascribed the low field peak to acidic OH groups coordinated to two Ti atoms, localized on bridging oxygen atoms and forming weak hydrogen bond adjacent to oxygen atoms; while the high field peak belongs to basic OH groups where hydrogen atoms are bound to terminal oxygen atoms. According to Jonsen,⁵¹ the sharp, small and narrow resonance implies that the hydrogen concentration is relatively low and these hydrogen species are situated in dynamically static and isolated interstitial sites within the oxide lattice. Otherwise, the broad signal involves hydroxyl protons and labile interstitial protons (surface and/or bulk), which experience extensive dynamic averaging. The shifting towards lower field and linewidth broadening of these signals are obvious for TiO_{2-x}@H₂ while the signal of terminal Ti-OH drastically increases. Two additional resonances at 3.68 (C) and 0.28 ppm (D) can be reasonably attributed to titanol groups located at internal defect sites.⁴¹ These groups can be ascribed to the H located in the disordered phase upon hydrogenation.^{34,35} Annealing the HGT composite under two different environments induces different surface hydroxy/hydroxylated species: H₂/Ar mixture gives a strong, broad resonance at 5.49 ppm and a sharp, small one at 0.38 ppm whereas three intense resonances at 5.35, 3.44 and 0.83 ppm are recorded for pure H₂ atmosphere. The resonances over HGT composites with upfield shifting due to the higher electronegativity of carbon atoms can be the superposition of additional carbonaceous component apart from TiO_{2-x}. The resonance in the range of $\delta =$

5.5-5.8 ppm can be tentatively assigned to -CH protons and aromatic protons which arise from carbonaceous species and are essentially immobile as a result of strong interaction with the structure; whilst the signals at 3.90 ppm and 1.28 ppm can be assigned to the tertiary C-O-H group and aliphatic protons (-CH₃ methyl, -CH₂ methylene).^{52,53} These resonances in HGT composites are most likely overlapping with strong signals of TiO_{2-x} due to its minority in mass composition. It is noteworthy that the hydrogenation dramatically reflects the alteration in hydrogen-bonding network of the materials. Such structural changes upon H₂ reduction environments suggest different behavior in photocatalytic performance of these composite materials.

Morphological studies – SEM and TEM

The local morphologies of blank and composite materials were investigated by electron microscopy. Typical SEM and TEM images of HGT composites are displayed in Fig. 3. Fig. 3B clearly shows TiO_{2-x} particles well distributed on HG layer in HGT@H₂/Ar. The inverted FFT images identify the fringe disorder along with the lattice expansion, $d_{101} = 0.378$ nm, compared to either TiO₂ or TiO_{2-x}. As shown in Fig. S4 (Supporting Information), well-resolved lattice fringes with interplanar spacings of 0.348

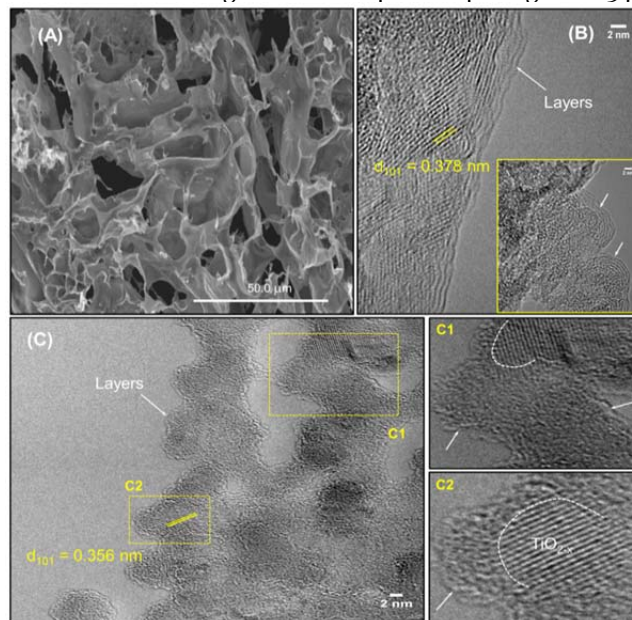
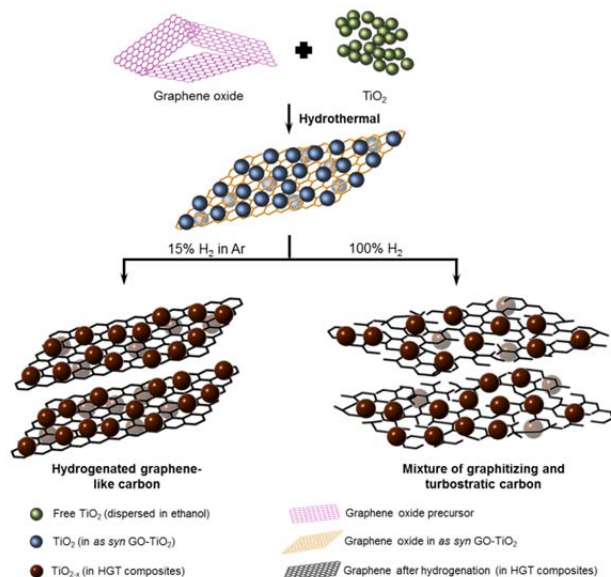


Figure 3. (A) SEM and (B) TEM micrograph of HGT@H₂/Ar and (C) TEM image along with local enlarged images of HGT@H₂. Inset of (B) is the image taken at specific edge showing different geometry of HGT@H₂/Ar.



Scheme 1. Illustration of topotactic transformation from hydrogenated graphene-like structure to mixture of graphitizing- and non-graphitizing carbon as annealing GO/TiO₂ composite under different H₂ atmosphere.

and 0.347 nm are revealed in TiO₂ and TiO_{2-x}, respectively, corresponding to the d-spacing of the (101) plane of anatase which is consistent with XRD results. It is obvious that the absence of a highly disordered layer at the outer shell of the particles as annealed under pure H₂ is inconsistent with some previous reports.^{32,34} Some part of the image become blurred and lattice disorder and dislocation occurs instead, as can be seen in the plot profile of lattice fringe in Fig. S4C-D. Meanwhile, the existence of few curled layers of HG (3-5 layers, visible interplanar spacing of 0.52 nm) surrounding TiO_{2-x} particles and highly disordered carbon layers are additionally detected at some specific edges as indicated in the inset of Fig. 3B. It can be relevant to the chemical bonding interaction (electrostatic and van der Waals interactions) and intimate interfacial contact between hydroxyl groups on the TiO₂ surface and abundant oxygen-containing functional groups on the basal planes and at the edges of the GO precursor. It is well accepted that due to such an abundance of these hydrophilic functional groups, GO acts as “a big macromolecular surfactant”, not only well dispersing in aqueous phase but also offering a large quantity of reactive sites to sufficiently interact with TiO₂.¹⁴ Such HG-wrapped TiO_{2-x} structure may be a beneficial factor to the charge transfer and separation from TiO₂ to the carbonaceous layers.

More importantly, such unique geometry is exclusively obtained over HGT composites annealed in high purity H₂ as shown in Fig. 3C. The lattice relaxation is also observed in TiO_{2-x} with $d_{101} = 0.356$ nm (also see in Fig. S5 and S6 in Supporting Information). Thin layers of HG almost disappear; instead the highly disordered carbon or turbostratic carbon in a wormhole-like structure is achieved. Turbostratic carbons, the intermediate between the ideal

graphite and amorphous carbon materials, are built up by nano-scale imperfect graphite crystallites, arranged almost parallel to one another, but with random orientation.⁵⁴⁻⁵⁷ Some regions of turbostratic structure consist of small packets of three-dimensionally (3D) ordered materials with disordering between packets, *i.e.*, the hollow-like central regions surrounded by graphitic layers.⁵⁵ Similar crystalline-to-amorphous, order-to-disorder transformation and reversed process have been reported where the co-existence of sp^2 - and sp^3 -bonded carbon atoms are observed.⁵⁸⁻⁶⁰ The presence of highly disordered carbon or turbostratic carbon in the HGT@H₂ composite is coincident with the Raman results where lower I_D/I_G was obtained. The carbonaceous component in terms of either hydrogenated graphene or a mixture of graphitic-like and turbostratic carbon obviously works as a grain boundary barrier, retarding the growth of anatase grain crystallites and thus leading to diminished crystallite sizes in comparison with TiO₂ and TiO_{2-x} as evident from XRD. Thus, in our study, as illustrated in Scheme 1, in the presence of TiO₂, the reduction in an H-rich atmosphere results in a topotactic transformation from hydrogenated graphene-like structure to mixture of graphitizing- and non-graphitizing carbon.

Electronic properties and chemical states – XPS analysis

Further understanding of the electronic and chemical nature of the carbon and TiO_{2-x} in HGT composites was unraveled by means of synchrotron XPS spectroscopy (Fig. 4). Three distinguishable photoelectron peaks at binding energies of ca. 284.6, 458 and 531 eV in the survey spectra (Fig. S7 in Supporting Information) are assigned to C 1s, Ti 2p and O 1s. Core-level Ti 2p and O 1s spectra are measured to gain insight into the surface structure of Ti and O species. As depicted in Fig. 4A, two spin-orbital splitting Ti 2p_{3/2} and Ti 2p_{1/2} peaks at 458.4-458.6 and 464.2-464.4 eV in blank and composite materials implicates the Ti⁴⁺ chemical state. The peak broadening might

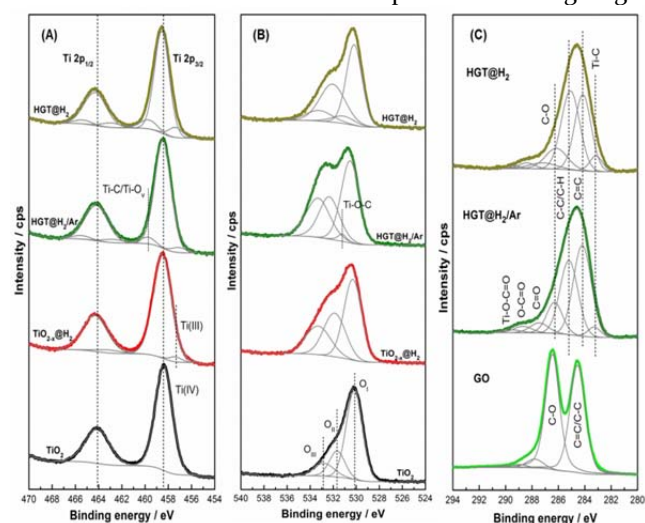


Figure 4. High resolution core-level XPS spectra of TiO₂, TiO_{2-x}@H₂ and HGT composites: (A) Ti 2p, (B) O 1s and (C) C 1s (peak fitting on Shirley backgrounds).

be due to either the interaction between TiO_{2-x} and HG, resulting in Ti-C bonding or the formation of oxygen vacancy upon hydrogenation (resolved into two peaks at 459.5-460.2 and 465.3-466.0 eV). However, very small features at 457.3-457.5 eV in the fitted spectra for $\text{TiO}_{2-x}@\text{H}_2$ and both HGT samples can be attributed to lower the asymmetrical profile in pristine TiO_2 , denoted as (i) oxidation state, Ti^{3+} . The existence of Ti^{3+} implicates the generation of oxygen defects in these samples, in particular, oxygen vacancies, to balance the charge compensation. The bonding environment of oxygen is shown in Fig. 4B. Three components of oxygen atoms are fitted from crystal lattice oxygen species O^{2-} (O_I , 530.1 eV); (ii) oxygen vacancy defect or surface low-coordinated oxygen ions, i.e. O_2^- , O_2^{2-} , O^- , CO_3^{2-} (O_{II} , 531.8 eV); (iii) hydroxyl-type oxygen species (OH^-) and surface-adsorbed molecular water (H_2O or O^{6-}) (O_{III} , 533.0 eV).⁶¹ It has been acknowledged that the physical adsorbed hydroxyl groups on TiO_2 can be easily removed under ultrahigh vacuum conditions typical of XPS measurements, the O_{II} and O_{III} peaks can be indeed originated from the species associated with the surface defects or strongly bound to surface defects on TiO_2 . It is clear that the O_{II} and O_{III} features developed with hydrogenation and HG addition, which possibly attributes to the shortage of oxygen in a reducing atmosphere. As summarized in Table 1, the relative (O_{II}/O_I) and ($\text{O}_{III}/\text{O}_I$) area ratios drastically increases from 0.277 to 0.595 and 0.760 for $\text{HGT}@\text{H}_2/\text{Ar}$ and $\text{HGT}@\text{H}_2$, respectively, indicating the generation of oxygen defects. Additionally, the small peak located at 531.0-531.2 eV in HGT composites is assignable to Ti-O-C bonding due to the chemical interaction between metal oxide and the carbonaceous material.¹⁷ The peak shift to higher binding energy along with an increment in relative (O_{II}/O_I) and ($\text{O}_{III}/\text{O}_I$) peak area ratios in TiO_{2-x} and HGT composites identifies the hydroxylated or oxyhydroxylated surface, resulting in the introduction of large amount of negatively charged oxygen vacancies. Similar phenomena can be found in the literature.^{62,63} The presence of these defect sites probably affects the separation of induced electrons/holes and charge transfer, as well as the photocatalytic performance.

The high resolution C 1s spectra in Fig. 4C can be deconvoluted into several components, including sp^2 -C bonds of the graphene skeleton (C=C, 284.2 eV), sp^3 -hybridized carbons (C-C/C-H, 285.2 eV), alcohol, epoxy and ether groups (C-O, 286.3 eV), carbonyl groups (C=O, 287.5 eV) and carboxylic acid/ester groups (O-C=O, 288.8). Compared to the pristine GO, the peak intensities of C-O, C=O and O-C=O substantially diminish, implicating that GO was almost reduced to HG through the hydrothermal and subsequent hydrogenation processes. The larger the amount of residual O-containing functional groups, the lower the conductivity of HG. Interestingly, the sp^3 -bonded C dominates, occupying 39.74% of the C concentration, as reduced HGT composite in an H-rich atmosphere. As shown in Table 2, the relative area ratio of C-C/C-H (sp^3 -carbon) and C=C (sp^2 -carbon) strongly increases from 0.826 to 1.155. Our results are in agreement

with the literature on hydrogenated graphene, graphone and graphene.^{30,48} The presence of well-defined C-O bonds after hydrogenation is in agreement with Wang et al.'s computations⁶⁴ that studied the hydrogenation of epoxy on the surface of graphene oxide by H_2 not only converts it into a hydroxyl but also simultaneously transforms an sp^2 carbon to sp^3 carbon. Two features centered at 283.2 and 289.6 eV correspond to Ti-O-C=O and Ti-C due to the strong coupling (covalent interaction) between TiO_{2-x} and HG.^{12,20,21} Specially, the dominance of Ti-C bonds (5.43%) in $\text{HGT}@\text{H}_2$ clearly indicates the close interconnection between TiO_{2-x} and carbonaceous layers.

Based on TEM, XPS and Raman spectra, it is plausible to suggest that in the presence of TiO_2 nanoparticles, GO sheets can undergo a topotactic transformation from graphitic carbon (honeycomb-like structure) to a mixture of graphitic and turbostratic carbon (amorphous/disordered) as altering the calcination atmosphere from a mild to an H-abundant environment. XRD/PDF, NMR, Raman and XPS results also imply there are remarkable changes in structure and chemical bonding states of TiO_2 , accompanied with the strong electronic communication between o-1D metal oxide and 2D carbon

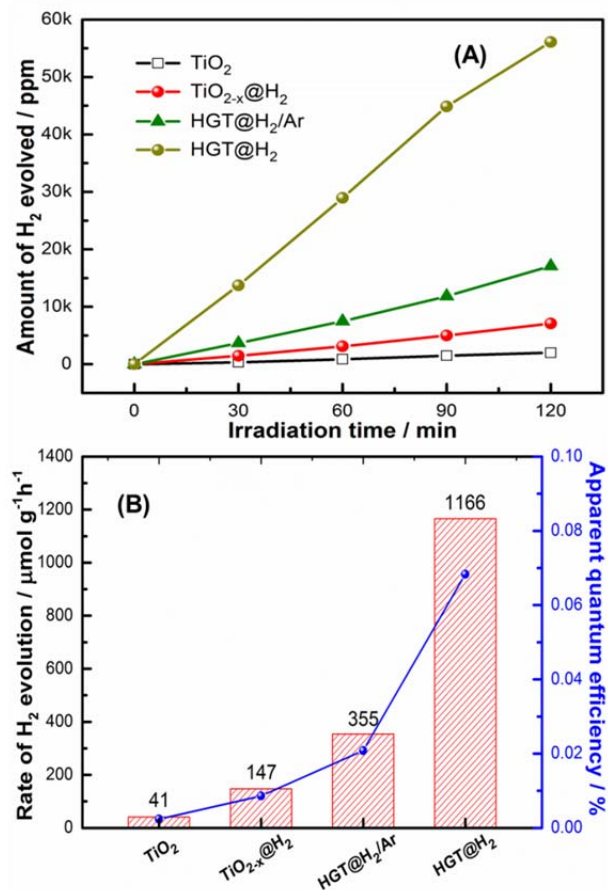


Figure 5. (A) Time curve of H_2 production and (B) mass-normalized evolution rates and quantum efficiencies over TiO_2 , $\text{TiO}_{2-x}@\text{H}_2$ and hydrogenated graphene/ TiO_{2-x} composites, respectively (aqueous methanol 20 vol% as sacrificial agent, 150 W Xenon arc lamp equipped with CuSO_4 filter at 293 K).

layers upon hydrogenation through the formation of Ti-C/Ti-O-C bonds and thus, an interfacial contact between them. Such differences in textural, structural and electronic properties possibly impact the migration efficiency of photoinduced electrons, the interfacial electron transfer and the charge recombination of HGT composites that are strongly relevant to the photocatalytic H₂-evolution activity.

Photocatalytic H₂ and O₂ evolution measurements

Fig. 5 compares the H₂ generation performance between HGT composites, TiO_{2-x}@H₂ and TiO₂, irradiated by the full output of a Xe lamp equipped with CuSO₄ filter (310 < λ < 625 nm) without the use of a noble metal co-catalyst. The time course of the reaction in Fig. 5A shows the proportional increase in the evolved H₂ overtime for each sample. It is clear that the presence of HG drastically accelerates the generation of H₂ under UV-visible light. As shown in Fig. 5B, the mass specific activity of reduced titania (147 μmol g⁻¹ h⁻¹) is ca. 3.5-time higher than that of air-treated TiO₂ (41 μmol g⁻¹ h⁻¹), possibly arising from the downward shift of the conduction band or the existence of a mid-gap state that is lower than reduction potential of H⁺/H₂ by the introduction of defects through hydrogenation.³² Chen et al.³² described that the energy

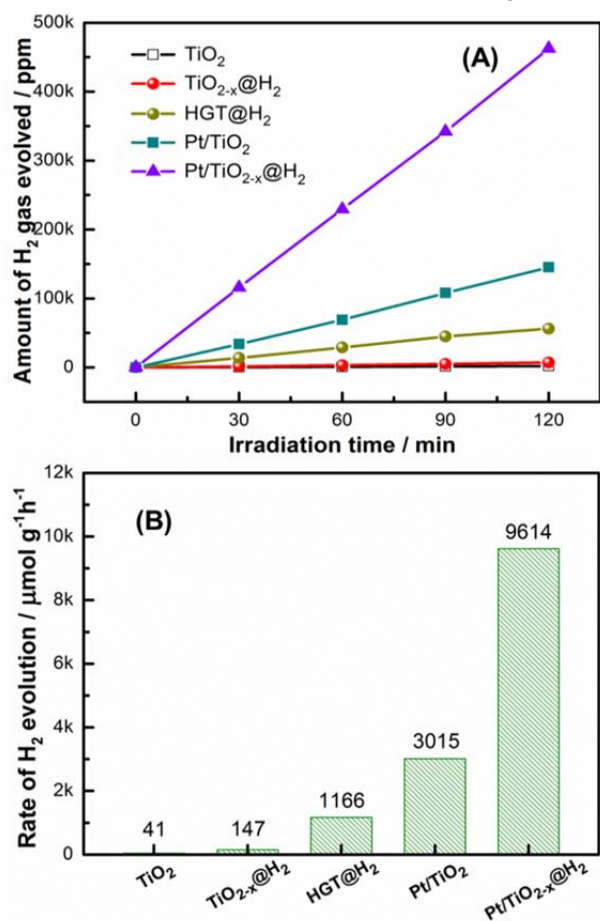


Figure 6. Comparison of H₂ evolution between Pt nanoparticles and hydrogenated graphene co-catalysts on TiO₂ and TiO_{2-x}@H₂ in aqueous methanol solution (150 W Xenon arc lamp equipped with CuSO₄ filter at 293 K).

distribution of mid-gap states differed from that of a single defect in a crystal, forming a continuum extending to and overlapping with the conduction band edge (known as band tail states). These band tail states merge with the valence band, extending the energy states. These defects also serve as trapping sites, preventing the charge carriers from the rapid recombination and improving the electron transfer, and hence the photocatalytic performance. The H₂ evolution rate is further enhanced to 355 μmol g⁻¹ h⁻¹ by the addition of hydrogenated graphene. Interestingly, the rate of H₂ production over the HGT@H₂ composite is found to sharply increase to 1.166 mmol g⁻¹ h⁻¹, approximately 7.9 and 3.3 times higher than TiO_{2-x} and HGT composite annealed under 15% H₂ in Ar atmosphere, respectively.

One of the reasonable concerns is whether the HG itself can act as the hydrogen reservoir during hydrogen evolution. Herein, 3 mg of HGT@H₂ generated ~ 7 μmol (14 μg) of H₂ after 2 h-irradiation. Assuming full coverage of hydrogen on graphene sheet by hydrogenation in pure H₂ atmosphere, each atomic hydrogen can hypothetically bond to each carbon atom. Thus, the maximum amount of hydrogen 'stored' in HGT@H₂ is 2.3 μg. It is noteworthy that in this study, the gas phase hydrogenation of GO/TiO₂ in H₂-enriched environment at 20 psi does not produce fully hydrogenated graphane (as proven by XPS and Raman). Both experimental reports and DFT calculations on hydrogenated graphene estimated the hydrogenation efficiency of < 10 at% even under hydrogen plasma.²⁹ Thus, the amount of evolved H₂ during catalysis is much greater than the amount of hydrogen potentially 'stored' in the composite. Based on these considerations hydrogenated GO support can be safely eliminated as the potential source of hydrogen gas produced during photocatalysis.

The apparent quantum efficiency (QE), which is given by the ratio between the moles per second of hydrogen produced and the moles (einsteins) of photons per second,⁶⁵⁻⁶⁷ for these materials was also calculated (see detail in Supporting Information). In some studies of photocatalytic water splitting over metal oxides and composite materials, the QE at a specific wavelength (monochromatic radiation) was reported whereas the reaction has been conducted under broadband radiation (polychromatic irradiation).^{12,68,69} Other strategy has been the combination of band-pass and cutoff filters to determine QE over narrow bandwidth or over maxima band.^{70,71} Herein, based on the calculation over the spectral range of 310-625 nm as shown in Fig. 5B, 0.068% and 0.021% were obtained for HGT@H₂ and HGT@H₂/Ar composites, much greater than TiO_{2-x} (0.0086%) and TiO₂ (0.0024%). QE of 0.102% was achieved for HGT@H₂ as calculated over the wavelength of 400-625 nm when using both CuSO₄ and 400 nm long pass filter (see Table S1 and S2 in Supporting Information).

It is apparent that the reduction in H₂-rich atmosphere shows a remarkable improvement in photocatalytic performance *via* the highest hydrogenation extent. Considering several other GP/TiO₂ composites synthesized and

reduced by different methods,¹⁰⁻²¹ due to the higher work function, $\Phi_{\text{GP}} = -4.42$ eV (vs. vacuum) and $\Phi_{\text{TiO}_2} = -4.2$ eV,^{16,72} GP acts as the electron acceptor and conductor to capture and shuttle photoexcited electrons from the conduction band of TiO_2 , efficiently prolonging the lifetime and improving the mobility of electrons (whilst photo-generated holes are scavenged by the methanol sacrificial agent) and thus, facilitating H_2 production. Herein, it can be inferred that the carbonaceous layers irrespective of hydrogenated graphene, disordered or turbostratic carbon plays the identical role as GP. Mixture of graphitizing- and turbostratic carbon enhances the strong interactions and maximizes the intimate interfacial contact between TiO_{2-x} nanoparticles and 2D carbonaceous layers, which favors the interfacial electron transport and efficiently retards the charge recombination. The other factors which may contribute to the enhanced performance will be discussed later.

It has been well established that the noble metal co-catalysts, *i.e.* Pt, Ru or Rh, are usually loaded onto the photocatalysts (with 0.5-1 wt%) to facilitate the photocatalytic water splitting performance because they enhance the separation of photogenerated electrons/holes, further improving the photocatalytic activity for proton production and water oxidation. However, tremendous efforts have been made in order to: (i) reduce the co-

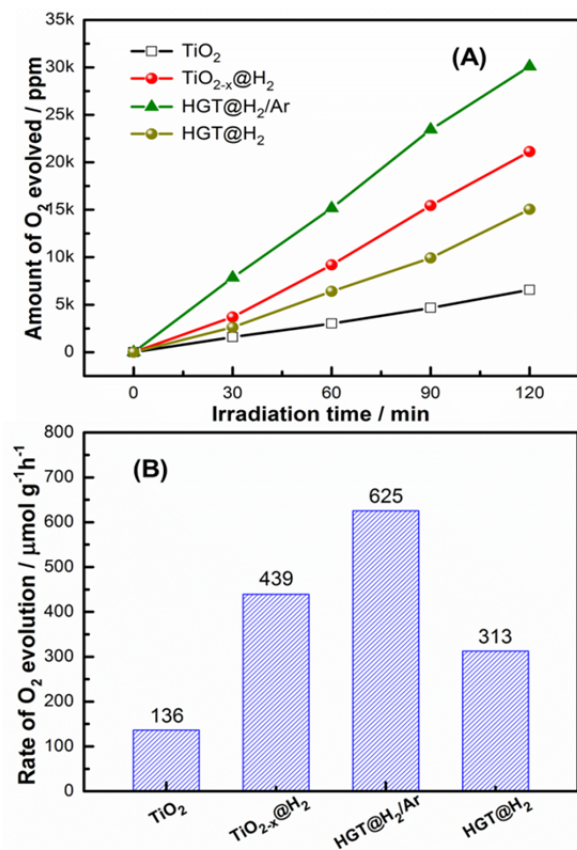


Figure 7. Light-driven O_2 production of TiO_2 , $\text{TiO}_{2-x}@\text{H}_2$ and $\text{HG}/\text{TiO}_{2-x}$ composites (aqueous AgNO_3 0.01 M as sacrificial agent, 150 W Xenon arc lamp equipped with CuSO_4 filter at 293 K).

catalyst content, (ii) replace noble metal co-catalyst with other abundant transition metals, (iii) explore potentially sustainable, cheap, efficient candidates to replace these noble metals, especially Pt, due to its extremely high cost and scarcity. Carbonaceous materials have been considered as promising alternatives to noble metal co-catalysts.³⁻⁹ Herein, the photocatalytic activity measurement under the presence of 1wt% Pt co-catalyst was conducted for comparison (Fig. 6). Pt nanoparticles were pre-loaded on *as-syn* TiO_2 by the impregnation method using H_2PtCl_6 as a metal precursor, followed by the calcination in either ambient air or high-purity H_2 atmosphere. The time course in Fig. 6A shows the enhanced activity of hydrogen production over the samples containing Pt nanoparticles. The H_2 evolution rate achieves 3.015 $\text{mmol g}^{-1} \text{h}^{-1}$ over Pt/TiO_2 sample as seen in Fig. 6B, approximately 73.5-times higher than that for blank sample (41 $\mu\text{mol g}^{-1} \text{h}^{-1}$). The rate exceeds 9.614 $\text{mmol g}^{-1} \text{h}^{-1}$ with Pt/TiO_2 samples hydrogenated under a H_2 -rich environment. The activity is 3.2-, 65.4- and 234.5-times of that obtained from Pt/TiO_2 , $\text{TiO}_{2-x}@\text{H}_2$ and bare TiO_2 , respectively. Due to greater work function of Pt (-5.64 eV),⁷³ the photoinduced electron transfer from the TiO_2 conduction band to Pt is energetically favorable and the holes are localized within TiO_2 , therefore effectively increasing charge carrier separation and then making the electrons accessible for proton reduction to form H_2 . It has been reported recently by Zhu et al⁷⁴ that such superior activity may be attributed to the involvement of hydrogen spillover from Pt to TiO_2 that greatly enhanced the catalytic activity. It is interesting to notice that the H_2 evolution rates of $\text{Pt}/\text{TiO}_{2-x}@\text{H}_2$ and Pt/TiO_2 are only 8.2- and 2.6-time higher than that of $\text{HGT}@\text{H}_2$, respectively, with the same nominal loading amount of GO and Pt (1 wt%). Thus, in order to reach same activity as $\text{Pt}/\text{TiO}_{2-x}@\text{H}_2$ and Pt/TiO_2 , hypothetically 2.5 ~ 8.5 wt% of GO precursor should be used. This simple comparative analysis demonstrates the potential of hydrogenated graphene-based TiO_2 composites to successfully rival the noble-metal-based photocatalysts.

On the other hand, oxidative half-reaction of overall water splitting - the water oxidation has been acknowledged to be much more challenging than H_2 production due to the consumption of four positive holes to oxidize water to oxygen and more stringent energetic requirements. As shown in Fig. 7, the hydrogenated titania creates 439 μmol of O_2 per hour per gram of catalyst, which is 3.2-fold higher than that over TiO_2 . This enhancement possibly implies that the hydrogenation significantly impacts the valence band structure of TiO_2 where the water oxidation takes place. However, the presence of hydrogenated graphene under H_2/Ar flow slightly enhances the O_2 performance, generating 625 $\mu\text{mol g}^{-1} \text{h}^{-1}$, whereas post treatment by pure H_2 makes the composite worse than TiO_{2-x} towards water oxidation (313 $\mu\text{mol g}^{-1} \text{h}^{-1}$).

Apart from the mass normalization for catalyst effectiveness, it has been known that the normalization of the catalytic activity (*i.e.* the rate of gas evolution) to photoactive surface sites (such as specific surface area or number of exposed photoactive sites) further provides a better

Table 3. Comparison of photocatalytic activity of different graphene-based catalysts for hydrogen generation.

Photocatalysts	Light source	Additive /Co-catalyst	Sacrificial electron donor	Rate of H ₂ evolution / $\mu\text{mol g}^{-1} \text{h}^{-1}$	Quantum efficiency / %	Refs.
Graphene/TiO ₂	500 W Xe lamp	- 5 wt% graphene - No noble-metal-co-catalyst	0.1 M Na ₂ S-0.04 M Na ₂ SO ₃	- UV-visible: 86 - Visible: not reported	Not reported	10
3D graphene/TiO ₂ hydrogel	300 W Xe lamp 420 nm cutoff filter	- 10 wt% graphene - 8 wt% Au co-catalyst	10% (v/v) CH ₃ OH-H ₂ O	- UV-visible: 51 (without Au) 242 (with Au) - Visible: 58 (without Au) 100 (with Au)	Not reported	18
Ag/graphene/P25	Xe lamp	- 5 wt% graphene - 1.5 wt% Ag co-catalyst	10% (v/v) CH ₃ OH-H ₂ O	- UV-visible: 210 (without Ag) 353 (with Ag) - Visible: not reported	Not reported	20
Graphene/TiO ₂ nanosheet	350 Xe arc lamp	- 1 wt% graphene - No noble-metal-co-catalyst	25% (v/v) C ₂ H ₅ OH-H ₂ O	- UV-visible: 736 - Visible: not reported	3.1% (at 365 nm – four 3W-UV LED lamps)	12
Reduced graphene oxide/P25	200 W Xe arc lamp	- 20wt% RGO - No noble-metal-co-catalyst	20% (v/v) CH ₃ OH-H ₂ O	- UV-visible: 740 - Visible: not reported	Not reported	11
Au/graphene/P25	High-pressure 400 W Hg lamp	- 1 wt% graphene - 2 wt% Au co-catalyst	10% (v/v) CH ₃ OH-H ₂ O	- UV-visible: 1340 (without Au) 12000 (with Au)	Not reported	19
Ag/graphene/P25	Xe lamp	- 5 wt% graphene - 1.5wt% Ag co-catalyst	10% (v/v) CH ₃ OH-H ₂ O	- UV-visible: 210 (without Ag) 353 (with Ag) - Visible: not reported	Not reported	20
Hydrogenated graphene/TiO_{2-x}	150 W Xe arc lamp equipped with CuSO₄ filter 400 nm cut-off filter	- 1wt% hydrogenated graphene - No noble-metal-co-catalyst	20% (v/v) CH₃OH-H₂O	- UV-visible: 1166 - Visible: 19	0.068% (310 ~ 625 nm)	This work
Cu/graphene/P25	300 W high pressure Hg lamp	- 2 wt% graphene - 1.5wt% Cu as co-catalyst	33% (v/v) CH ₃ OH-H ₂ O	- UV-visible: 12500 (without Cu) 65600 (with Cu) - Visible: not reported	Not reported	13
Vacuum-activated graphene/self-doped TiO ₂	300 W Xe arc lamp/ 400 nm cutoff filter	- 2wt% graphene - 0.37 wt% Pt co-catalyst	20% (v/v) CH ₃ OH-H ₂ O	- UV-visible: not reported - Visible: 4000	Not reported	21

understanding of bulk and surface structural variations due to strong sensitivity to both crystallinity of the bulk lattice and surface features.^{65,75} Fig. 8A shows the corresponding BET surface area normalized turnover rate of H₂ and O₂ production. As shown in Table 1, HGT@H₂/Ar possesses large surface area (> 120 m² g⁻¹) which can be attributed to the smaller average crystallite size and the presence of stacked HG layers previously elucidated by XRD and TEM. Consequently, the result clearly indicates the negative effect of the HG additive on O₂ production after normalization to surface area. Reduced titania itself exhibits the highest O₂ evolution rate, ~ 7.8 μmol m² h⁻¹. It is clear that either hydrogenated graphene or a mixture of HG and turbostratic carbon is not optimal candidates for photocatalytic water oxidation. It can be ascribable to the surface oxygen vacancies which are not stable and even susceptible to oxidation by dissolved oxygen in water; in contrast, the oxygen vacancies in the bulk can avoid the interaction with O₂.³⁵ It is proposed that due to a large concentration of oxygen defects in the HGT composites, the fraction of bulk oxygen vacancies can be much higher than the others, possibly leading to lower O₂ evolution. Otherwise, slightly enhanced H₂ turnover rate of this composite (2.9 μmol m² h⁻¹) is observed compared to hydrogenated titania (2.6 μmol m² h⁻¹). Herein, the highest reactivity is obtained for the HGT composite reduced in a rich-H₂ environment, 15.6 μmol m² h⁻¹.

The photocatalytic H₂ evolution of all samples under

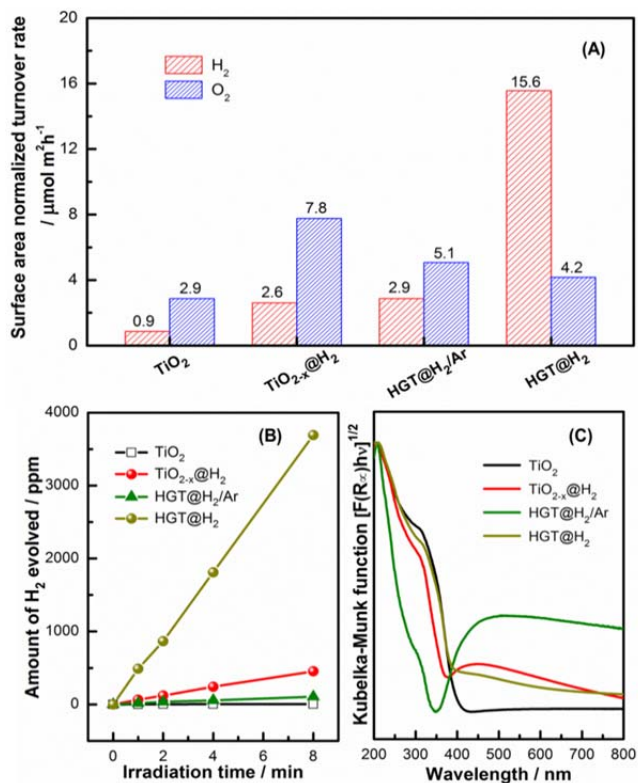


Figure 8. (A) Surface-area-normalized activity of H₂ and O₂ production, (B) visible-light-driven H₂ evolution (150 Xe arc lamp, CuSO₄ and 400 nm cutoff filter), and (C) UV-vis-DRS spectra of blank and composite materials.

visible light irradiation was also studied by using a 400 nm long pass filter ($400 < \lambda < 625$ nm). As seen in Fig. 8B, compared to blank TiO₂ with no activity, TiO_{2-x}@H₂ produces 454 ppm of H₂ after 8 h of illumination, corresponding to the rate of 2.4 μmol g⁻¹ h⁻¹. HGT@H₂ composite exhibits an increased hydrogen evolution rate of 19.2 μmol g⁻¹ h⁻¹ (generating 3692 ppm of H₂ gas), whereas HGT@H₂/Ar shows much lower activity even compared to reduced titania. Generally, the photocatalytic gas production over HGT composites is strongly affected by the reduction environment and the diverse photocatalytic performance may be associated with several factors. One of the most important factors is the optical properties of the materials. Fig. 8C illustrates the diffuse reflectance UV-Vis spectra of TiO₂, TiO_{2-x}@H₂ and HGT composites. Comparison with air-calcined TiO₂, which only responds under the UV region, the reduced ones are optically absorbing the visible-light region from 380 to 800 nm, along with the blue-shift of the absorption edge. Interestingly, the HGT@H₂/Ar composite exhibits unusual optical behavior where the onset is located at 350 nm and a broad, strong absorption up to 800 nm is observed. However, the edge red-shifts as reducing HGT material in pure H₂, extending the photoresponse into the visible range up to 800 nm. It implies that annealing the composite materials under different reducing atmospheres induces different photocatalytically reactivity, probably originated from the formation of Ti-C/Ti-O-C bonds due to a strong interaction between TiO_{2-x} and HG which was proven by XPS spectra above. That explains the highest visible-light-driven H₂ evolution over HGT@H₂ composite. Indeed, no rational explanation of the blue-shift is explored in this study; nevertheless, as mentioned above, the band gap of graphene can be easily tuned from a small indirect band gap to a wide direct band gap *via* the manipulation of the hydrogen reduction.²⁴ Therefore, the different nature of carbon structures in the composites possibly leads to different optical properties. The coupling between HG and TiO_{2-x} requires further analysis and study to clarify a mechanistic pathway.

It is also worth noting that such differences in photocatalytic performance can be partially ascribed to the introduction of abundant defects and different carbon speciation under different hydrogenation conditions. The hydrogenation-induced oxygen vacancies (as confirmed by XPS analysis) can behave as an electron donor and significantly increase the donor density in TiO_{2-x}, thus possibly improving the charge transport. Similar phenomena have been demonstrated on hydrogenated titania in several previous reports.³²⁻³⁴ High separation efficiency of majority and minority carriers due to surface oxygen vacancies and Ti³⁺ centers is an important factor. The oxygen vacancies work as electron traps while Ti³⁺ sites acts as hole scavengers, both accompanied with the role of adsorption sites where the charge transfer to adsorbed species can prevent the recombination of electron-hole pairs, whereas bulk defects only act as charge carrier traps where electron-holes recombine.³⁶ Additionally, the HG can play the role of an electron shuttle, transferring the

photogenerated electrons from conduction band of TiO_{2-x} to the HG- TiO_{2-x} interface and eventually to HG conductor, facilitating the separation of electron/hole pairs at the interface, and subsequently reducing protons to produce H_2 .¹⁰⁻²¹ Improved performance of hydrogenated composites for the light-driven water reduction half-reaction can be attributed to the synergistic effect between the generated defects and emerged graphitic-/turbostratic carbon structure which contains more defects and sp^3 -bonded carbon.

The comparison of photocatalytic performance of the HGT composite and different catalytic materials reported in the literature using either graphene or noble metal as additives or co-catalysts is shown in Table 3. The rate of H_2 production and quantum efficiency are two important values to evaluate the potential of a photocatalyst. The performance of HGT composites reported in this study is quite impressive compared with the photocatalysts in previous reports. Although more mechanistic studies are further needed to establish better understanding of photophysical and catalytic properties of the HGT composites, while the findings of the present study provide new insights into the development of the coupling of metal oxides with graphone or graphane to exploit numerous new potential applications.

CONCLUSION

We have investigated the role of hydrogenation on the structure, electronic properties and photocatalytic activity of hydrogenated graphene/ TiO_{2-x} composites. The hydrogenation not only reduces TiO_2 nanoparticles but also impacts the graphene-like structure in the composites. GO sheets undergo a topotactic transformation from a graphene-like structure to a mixture of graphitic and turbostratic carbon (amorphous/disordered) when altering the calcination atmosphere from a mild to H-abundant environment. The composite annealed upon H-rich conditions exhibits the highest H_2 evolution performance whereas the mild reduction shows a slight improvement in O_2 production. Such enhancement can be attributed to the introduction of large amount of oxygen vacancies and Ti^{3+} states, retarding the recombination of charge carriers and thus, facilitating the charge transfer from TiO_{2-x} to the carbonaceous sheet. The findings of the present study may open up an exciting opportunity for developing new strategies for coupling metal oxides with graphone or graphene to replace existing noble metal-based photocatalysts.

ASSOCIATED CONTENT

Supporting Information. Includes the synthesis procedure of graphene oxide precursor, detail for the calculation of apparent quantum efficiency and 7 supporting figures (Figure S1 to S7) of lamp irradiance spectra, HR-TEM, PDF and XPS analyses. This material is available free of charge via the Internet at <http://pubs.acs.org>.

AUTHOR INFORMATION

Corresponding Author

* rodriguez@bnl.gov

Notes

The authors declare no competing financial interest.

ACKNOWLEDGMENT

The research carried out in this manuscript was performed at Brookhaven National Laboratory, supported by the U.S. Department of Energy, Office of Science, Office of Basic Energy Sciences, and Catalysis Science Program under contract No. DE-SC0012704. This work used resources of the National Synchrotron Light Source (NSLS) and the Center for Functional Nanomaterials (CFN), which are DOE Office of Science User Facilities. We would like to thank Dr. Viet Hung Pham (CFN) for Raman analysis.

REFERENCES

- (1) Novoselov, K. S.; Geim, A. K.; Morozov, S. V.; Jiang, D.; Zhang, Y.; Dubonos, S. V.; Grigorieva, I. V.; Firsov, A. A., Electric Field Effect in Atomically Thin Carbon Films. *Science* **2004**, *306*, 666-669.
- (2) Geim, A. K.; Novoselov, K. S., The Rise of Graphene. *Nat. Mater.* **2007**, *6*, 183-191.
- (3) Singh, V.; Joung, D.; Zhai, L.; Das, S.; Khondaker, S. I.; Seal, S., Graphene based Materials: Past, Present and Future. *Prog. Mater. Sci.* **2011**, *56*, 1178-1271.
- (4) Wu, Z.-S.; Zhou, G.; Yin, L.-C.; Ren, W.; Li, F.; Cheng, H.-M., Graphene/Metal Oxide Composite Electrode Materials for Energy Storage. *Nano Energy* **2012**, *1*, 107-131.
- (5) Wang, S; Sun, H.; Ang, H. M.; Tadé, M. O., Adsorptive Remediation of Environmental Pollutants using Novel Graphene-based Nanomaterials. *Chem. Eng. J.* **2013**, *226*, 336-347.
- (6) Lightcap, I. V.; Kamat, P. V.; Graphitic Design: Prospects of Graphene-Based Nanocomposites for Solar Energy Conversion, Storage, and Sensing. *Acc. Chem. Res.* **2013**, *46*, 2235-2243.
- (7) Nardecchia, S.; Carriazo, D.; Ferrer, M. L.; Gutiérrez, M. C.; del Monte, F., Three dimensional Macroporous Architectures and Aerogels built of Carbon Nanotubes and/or Graphene: Synthesis and Applications. *Chem. Soc. Rev.* **2013**, *42*, 794-830.
- (8) Cao, X.; Yin, Z.; Zhang, H., Three-dimensional Graphene Materials: Preparation, Structures and Application in Supercapacitors. *Energy Environ. Sci.* **2014**, *7*, 1850-1865.
- (9) Chowdhury, S.; Balasubramanian, R., Recent Advances in the Use of Graphene-family Nanoadsorbents for Removal of Toxic Pollutants from Wastewater. *Adv. Colloid Interface Sci.* **2014**, *204*, 35-56.
- (10) Zhang, X.-Y.; Li, H.-P.; Cui, X.-L.; Lin, Y., Graphene/ TiO_2 Nanocomposites: Synthesis, Characterization and Application in Hydrogen Evolution from Water Photocatalytic splitting. *J. Mater. Chem.* **2010**, *20*, 2801-2806.
- (11) Fan, W.; Lai, Q.; Zhang, Q.; Wang, Y., Nanocomposites of TiO_2 and Reduced Graphene Oxide as Efficient Photocatalysts for Hydrogen Evolution. *J. Phys. Chem. C* **2011**, *115*, 10694-10701.
- (12) Xiang, Q.; Yu, J.; Jaroniec, M., Enhanced Photocatalytic H_2 -production Activity of Graphene-modified Titania Nanosheets. *Nanoscale* **2011**, *3*, 3670-3678.
- (13) Lv, X.-J.; Zhou, S.-X.; Zhang, C.; Chang, H.-X.; Chen, Y.; Fu, W.-F., Synergetic Effect of Cu and Graphene as Co-catalyst on TiO_2 for Enhanced Photocatalytic Hydrogen

- Evolution from Solar Water Splitting. *J. Mater. Chem.* **2012**, *22*, 18542–18549.
- (14) Zhang, Y.; Zhang, N.; Tang, Z.-R.; Xu, Y.-J., Improving the Photocatalytic Performance of Graphene-TiO₂ Nanocomposites via a Combined Strategy of Decreasing Defects of Graphene and Increasing Interfacial Contact. *Phys. Chem. Chem. Phys.* **2012**, *14*, 9167–9175.
 - (15) Sun, L.; Zhao, Z.; Zhou, Y.; Liu, L., Anatase TiO₂ Nanocrystals with Exposed {001} Facets on Graphene Sheets via Molecular Grafting for Enhanced Photocatalytic Activity. *Nanoscale* **2012**, *4*, 613–620.
 - (16) Morales-Torres, S.; Pastrana-Martínez, L. M.; Figueiredo, J. L.; Faria, J. L.; Silva, A. M. T., Design of Graphene-based TiO₂ Photocatalysts—a Review. *Environ. Sci. Pollut. Res.* **2012**, *19*, 3676–3687.
 - (17) Lu, T.; Zhang, R.; Hu, C.; Chen, F.; Duo, S.; Hu, Q., TiO₂-Graphene Composites with Exposed {001} Facets Produced by a One-pot Solvothermal Approach for High Performance Photocatalyst. *Phys. Chem. Chem. Phys.* **2013**, *15*, 12963–12970.
 - (18) Gao, M.; Peh, C. K. N.; Ong, W. L.; Ho, G. W., Green Chemistry Synthesis of a Nanocomposites Graphene Hydrogel with Three-dimensional Nanomesopores for Photocatalytic H₂ Production. *RSC Adv.* **2013**, *1*, 13169–13177.
 - (19) Singh, G. P.; Shrestha, K. M.; Nepal, A.; Klabunde, K. J.; Sorensen, C. M., Graphene Supported Plasmonic Photocatalyst for Hydrogen Evolution in Photocatalytic Water Splitting. *Nanotechnol.* **2014**, *25*, 265701.
 - (20) Yang, Y.; Liu, E.; Dai, H.; Kang, L.; Wu, H.; Fan, J.; Hu, X.; Liu, H., Photocatalytic Activity of Ag-TiO₂-Graphene Ternary Nanocomposites and Application in Hydrogen Evolution by Water Splitting. *Int. J. Hydrogen Energy* **2014**, *39*, 7664–7671.
 - (21) Qiu, B.; Zhou, Y.; Ma, Y.; Yang, X.; Sheng, W.; Xing, M.; Zhang, J., Facile Synthesis of the Ti³⁺ Self-doped TiO₂-Graphene Nanosheet Composites with Enhanced Photocatalysis. *Sci. Rep.* **2015**, *5*, 8591.
 - (22) Chen, X.; Mao, S. S., Titanium Dioxide Nanomaterials: Synthesis, Properties, Modifications, and Applications. *Chem. Rev.* **2007**, *107*, 2891–2959.
 - (23) Muñoz-Batista, M. J.; Kubacka, A.; Fernández-García, M., Effective Enhancement of TiO₂ Photocatalysis by Synergistic Interaction of Surface Species: From Promoters to Co-catalysts. *ACS Catal.* **2014**, *4*, 4277–4288.
 - (24) Elias, D. D.; Nair, R. R.; Mohiuddin, T. M. G.; Morozov, S. V.; Blake, P.; Halsall, M. P.; Ferrari, A. C.; Boukhalov, D. W.; Katnelson, M. I.; Geim, A. K.; Novoselov, K. S., Control of Graphene's Properties by Reversible Hydrogenation: Evidence for Graphane. *Science* **2009**, *323*, 610–613.
 - (25) Zhou, J.; Wang, Q.; Sun, Q.; Chen, X. S.; Kawazoe, Y.; Jena, P., Ferromagnetism in Semihydrogenated Graphene Sheet. *Nano Lett.* **2009**, *9*, 3867–3870.
 - (26) Cadelano, E.; Palla, P. L.; Giordano, S.; Colombo, L., Elastic Properties of Hydrogenated Graphene. *Phys. Rev. B* **2010**, *82*, 235414.
 - (27) Sun, Z.; Pint, C. L.; Marcano, D. C.; Zhang, C.; Yao, J.; Ruan, G.; Yan, Z.; Zhu, Y.; Hauge, R. H.; Tour, J. M., Towards Hybrid Superlattices in Graphene. *Nat. Commun.* **2011**, *2*, 559.
 - (28) Shkrebtii, A. I.; Heritage, E.; McNelles, P.; Cabellos, J. L.; Mendoza, B. S., Graphene and Graphane Functionalization with Hydrogen: Electronic and Optical Signatures. *Phys. Status Solidi C* **2012**, *9*, 1378–1383.
 - (29) Pumera, M.; Wong, C. H. A., Graphane and Hydrogenated Graphene. *Chem. Soc. Rev.* **2013**, *42*, 5987–5995.
 - (30) Rajasekaran, S.; Abild-Pedersen, F.; Ogasawara, H.; Nilsson, A.; Kaya, S., Interlayer Carbon Bond Formation Induced by Hydrogen Adsorption in Few-Layer Supported Graphene. *Phys. Rev. Lett.* **2013**, *111*, 085503.
 - (31) Sofer, Z.; Jankovský, O.; Šimek, P.; Soferová, L.; Sedmidubský, D.; Pumera, M., Highly Hydrogenated Graphene via Active Hydrogen Reduction of Graphene Oxide in the Aqueous Phase at Room Temperature. *Nanoscale* **2014**, *6*, 2153–2160.
 - (32) Chen, X.; Liu, L.; Yu, P. Y.; Mao, S. S., Increasing Solar Absorption for Photocatalysis with Black Hydrogenated Titanium Dioxide Nanocrystals. *Science* **2011**, *331*, 746–750.
 - (33) Jiang, X.; Zhang, Y.; Jiang, J.; Rong, Y.; Wang, Y.; Wu, Y.; Pan, C., Characterization of Oxygen Vacancy Associates within Hydrogenated TiO₂: A Positron Annihilation Study. *J. Phys. Chem. C* **2012**, *116*, 22619–22624.
 - (34) Chen, X.; Liu, L.; Liu, Z.; Marcus, M. A.; Wang, W.-C.; Oyler, N. A.; Grass, M. E.; Mao, B.; Glans, P.-A.; Yu, P. Y.; Guo, J.; Mao, S. S., Properties of Disorder-Engineered Black Titanium Dioxide Nanoparticles through Hydrogenation. *Sci. Rep.* **2013**, *3*, 1510.
 - (35) Li, G.; Lian, Z.; Li, X.; Xu, Y.; Wang, W.; Zhang, D.; Tian, F.; Li, H., Ionothermal Synthesis of Black Ti³⁺-doped Single-crystal TiO₂ as an Active Photocatalyst for Pollutant Degradation and H₂ Generation. *J. Mater. Chem. A* **2015**, *3*, 3748–3756.
 - (36) Pan, X.; Yang, M.-Q.; Fu, X.; Zhang, N.; Xu, Y.-J., Defective TiO₂ with Oxygen Vacancies: Synthesis, Properties and Photocatalytic Applications. *Nanoscale* **2013**, *5*, 3601–3614.
 - (37) Su, J.; Zou, X.; Chen, J.-S., Self-modification of Titanium Dioxide Materials by Ti³⁺ and/or Oxygen Vacancies: New Insights into Defect Chemistry of Metal Oxides. *RSC Adv.* **2014**, *4*, 13979–13988.
 - (38) Wang, J.; Shen, L.; Nie, P.; Xu, G.; Ding, B.; Fang, S.; Dou, H.; Zhang, X., Synthesis of Hydrogenated TiO₂-Reduced-Graphene Oxide Nanocomposites and their Application in High Rate Lithium Ion Batteries. *J. Mater. Chem. A* **2014**, *2*, 9150–9155.
 - (39) Zhang, X.; Chen, Z., The Enhanced Photoactivity of Hydrogenated TiO₂@Reduced Graphene Oxide with p-n Junctions. *RSC Adv.* **2015**, *5*, 26328–26334.
 - (40) Larson, C.; Von Dreele, R. B., *General Structure Analysis System (GSAS)*. Los Alamos National Laboratory: Report LAUR, 1994, 86-748.
 - (41) Luo, S.; Nguyen-Phan, T.-D.; Johnston-Peck, A. C.; Barrio, L.; Sallis, S.; Arena, D.A.; Kundu, S.; Xu, W.; Piper, L. F. J.; Stach, E. A.; Polyansky, D. E.; Fujita, E.; Rodriguez, J. A.; Senanayake, S. D., Hierarchical Heterogeneity at the Ce-O_x-TiO₂ Interface: Electronic and Geometric Structural Influence on the Photocatalytic Activity of Oxide on Oxide Nanostructures. *J. Phys. Chem. C* **2015**, *119*, 2669–2679.
 - (42) Muscat, J.; Swamy, V.; Harrison, N. M., First-principles Calculations of the Phase Stability of TiO₂. *Phys. Rev. B* **2002**, *65*, 224112.
 - (43) Yu, P.Y.; Cardona, M., *Fundamentals of Semiconductors: Physics and Materials Properties*. Springer: Heidelberg, ed. 4, 2010.
 - (44) Sahoo, S.; Arora, A. K.; Sridharan, V., Raman Line Shapes of Optical Phonons of Different Symmetries in Anatase TiO₂ Nanocrystals. *J. Phys. Chem. C* **2009**, *113*, 16927–16933.
 - (45) Zheng, Z.; Huang, B.; Lu, J.; Wang, Z.; Qin, X.; Zhang, X.; Dai, Y.; Whangbo, M.-H., Hydrogenated Titania: Synergy of Surface Modification and Morphology Improvement for Enhanced Photocatalytic Activity. *Chem. Commun.* **2012**, *48*, 5733–5735.
 - (46) Ferrari, A. C.; Meyer, J. C.; Scardaci, V.; Casiraghi, C.; Lazzeri, M.; Mauri, F.; Piscanec, S.; Jiang, D.; Novoselov,

- K. S.; Roth, S.; Geim, A. K., Raman Spectrum of Graphene and Graphene Layers. *Phys. Rev. Lett.* **2006**, *97*, 187401.
- (47) Ai, K.; Liu, Y.; Lu, L.; Cheng, X.; Huo, L., A Novel Strategy for Making Soluble Reduced Graphene Oxide Sheets Cheaply by Adopting an Endogenous Reducing Agent. *J. Mater. Chem.* **2011**, *21*, 3365-3370.
- (48) Li, Y.; Chen, H.; Voo, L. Y.; Ji, J.; Zhang, G.; Zhang, G.; Zhang, F.; Fan, X., Synthesis of Partially Hydrogenated Graphene and Brominated Graphene. *J. Mater. Chem.* **2012**, *22*, 15021-15024.
- (49) Crocker, M.; Herold, R. H. M.; Wilson, A. E.; Mackay, M.; Emeis, C. A.; Hoogendoorn, A. M., ¹H NMR Spectroscopy of Titania. Chemical Shift Assignments for Hydroxy Groups in Crystalline and Amorphous Forms of TiO₂. *J. Chem. Soc., Faraday Trans.* **1996**, *92*, 2791-2798.
- (50) Chary, K. V. R.; Bhaskar, T.; Kishan, G.; Vijayakumar, V., Characterization of MoO₃/TiO₂ (Anatase) Catalysts by ESR, ¹H MAS NMR, and Oxygen Chemisorption. *J. Phys. Chem. B* **1998**, *102*, 3936-3940.
- (51) Jonsen, P., Identification of Different Hydrogen-Reduced Titania Crystallographic Forms by ¹H NMR Spectroscopy. *Catal. Lett.* **1989**, *2*, 345-350.
- (52) He, H.; Riedl, T.; Lerf, A.; Klinowski, J., Solid-State NMR Studies of the Structure of Graphite Oxide. *J. Phys. Chem.* **1996**, *100*, 19954-19958.
- (53) Ou, B.; Zhou, Z.; Liu, Q.; Liao, B.; Yi, S.; Ou, Y.; Zhang, X.; Li, D., Covalent Functionalization of Graphene with Poly(methyl methacrylate) by Atom Transfer Radical Polymerization at Room Temperature. *Polym. Chem.* **2012**, *3*, 2768-2775.
- (54) Warren, B. E., X-Ray Diffraction in Random Layer Lattices. *Phys. Rev.* **1941**, *59*, 693-698.
- (55) Badami, D. V.; Kaye, G., The Nature of Turbostratic Carbon. *Carbon* **1964**, *1*, 375-375.
- (56) Dasgupta, K.; Sathiyamoorthy, D., Disordered Carbon-Its Preparation, Structure, and Characterization. *Mater. Sci. Technol.* **2003**, *19*, 995-1002.
- (57) Li, Z. Q.; Lu, C. J.; Xia, Z. P.; Zhou, Y.; Luo, Z., X-ray Diffraction Patterns of Graphite and Turbostratic Carbon. *Carbon* **2007**, *45*, 1686-1695.
- (58) Shen, T. D.; Ge, W. Q.; Wang, K. Y.; Quan, M. X.; Wang, J. T.; Wei, W. D.; Koch, C. C., Structural Disorder and Phase Transformation in Graphite Produced by Ball Milling. *Nanostruct. Mater.* **1996**, *7*, 393-399.
- (59) Huang, J. Y., HRTEM and EELS Studies of Defects Structure and Amorphous-like Graphite Induced by Ball-Milling. *Acta Mater.* **1999**, *47*, 1801-1808.
- (60) Barreiro, A.; Börrnert, F.; Avdoshenko, S. M.; Rellinghaus, B.; Cuniberti, G.; Rummeli, M. H.; Vandersypen, L. M. K., Understanding the Catalyst-free Transformation of Amorphous Carbon into Graphene by Current-induced Annealing. *Sci. Rep.* **2013**, *3*, 1115.
- (61) Dupin, J.-C.; Gonbeau, D.; Vinatier, P.; Levasseur, A., Systematic XPS Studies of Metal Oxides, Hydroxides and Peroxides. *Phys. Chem. Chem. Phys.* **2000**, *2*, 1319-1324.
- (62) Naeem, M.; Hasanain, S. K.; Kobayashi, M.; Ishida, Y.; Fujimori, A.; Buzby, S.; Shah, S. I., Effect of Reducing Atmosphere on the Magnetism of Zn_{1-x}Co_xO Nanoparticles. *Nanotechnol.* **2006**, *17*, 2675-2680.
- (63) Mohanty, P.; Mishra, N. C.; Choudhary, R. J.; Banerjee, A.; Shripathi, T.; Lalla, N. P.; Annapoorni, S.; Rath, C., Oxygen Vacancy Induced Phase Formation and Room Temperature Ferromagnetism in Undoped and Co-doped TiO₂ Thin Films. *J. Phys. D: Appl. Phys.* **2012**, *45*, 325301.
- (64) Wang, L.; Lee, K.; Sun, Y.-Y.; Lucking, M.; Chen, Z.; Zhao, J. J.; Zhang, S. B., Graphene Oxide as an Ideal Substrate for Hydrogen Storage. *ACS Nano* **2009**, *3*, 2995-3000.
- (65) Braslavsky, S. E.; Braun, A. M.; Cassano, A. E.; Emeline, A. V.; Litter, M. I.; Palmisano, L.; Parmon, V. N.; Serpone, N., Glossary of Terms Used in Photocatalysis and Radiation Catalysis (IUPAC Recommendations 2011). *Pure Appl. Chem.* **2011**, *83*, 931-1014.
- (66) Serpone, N.; Salinaro, A., Terminology, Relative Photonic Efficiencies and Quantum Yields in Heterogeneous Photocatalysis. Part I: Suggested Protocol (Technical Report). *Pure Appl. Chem.* **1999**, *71*, 303-320.
- (67) Salinaro, A.; Emeline, A. V.; Zhao, J.; Hidaka, H.; Ryabchuk, V. K.; Serpone, N., Terminology, Relative Photonic Efficiencies and Quantum Yields in Heterogeneous Photocatalysis. Part II: Experimental Determination of Quantum Yields (Technical Report). *Pure Appl. Chem.* **1999**, *71*, 321-335.
- (68) Li, Q.; Guo, B.; Yu, J.; Ran, J.; Zhang, B.; Yan, H.; Gong, J. R., Highly Efficient Visible-Light-Driven Photocatalytic Hydrogen Production of CdS-Cluster-Decorated Graphene Nanosheets. *J. Am. Chem. Soc.* **2011**, *133*, 10878-10884.
- (69) Yu, J.; Yang, B.; Cheng, B., Noble-metal-free Carbon Nanotube-Cd_{0.1}Zn_{0.9}S Composites for High Visible-Light Photocatalytic H₂-Production Performance. *Nanoscale* **2012**, *4*, 2670-2677.
- (70) Zhang, J.; He, R.; Liu, X., Efficient Visible Light Driven Photocatalytic Hydrogen Production from Water using Attapulgite Clay Sensitized by CdS Nanoparticles. *Nanotechnol.* **2013**, *24*, 505401.
- (71) Bhunia, M. K.; Yamauchi, K.; Takanabe, K., Harvesting Solar Light with Crystalline Carbon Nitrides for Efficient Photocatalytic Hydrogen Evolution. *Angew. Chem. Int. Ed.* **2014**, *53*, 1-6.
- (72) Grätzel, M., Photoelectrochemical Cells. *Nature* **2001**, *414*, 338-344.
- (73) Lide, D. R., Ed., *CRC Handbook of Chemistry and Physics*. CRC Press: Florida, 90th ed., 2009.
- (74) Zhu, Y.; Liu, D.; Meng, M., H₂ Spillover Enhanced Hydrogenation Capability of TiO₂ Used for Photocatalytic Splitting of Water: A Traditional Phenomenon for New Applications. *Chem. Commun.* **2014**, *50*, 6049-6051.
- (75) Wachs, I. E.; Phivilay, S. P.; Roberts, C. A., Reporting of Reactivity for Heterogeneous Photocatalysis. *ACS Catal.* **2013**, *3*, 2606-2611.

Table of Contents (TOC)

